Available online at www.sciencedirect.com
ScienceDirect
Trans. Nonferrous Met. Soc. China 32(2022) 1935−1947
Transactions of Nonferrous Metals Society of China
www.tnmsc.cn

Preparation and properties of Ni-coated WC powder and highly impact resistant and corrosion resistant WC−Ni cemented carbides

Fan-lu MIN[1,2], Song-bai YU[3], Sheng WANG[2], Zhan-hu YAO[4],
Jacques Guillaume NOUDEM[5], Si-jin LIU[6], Jian-feng ZHANG[3]

1. Key Laboratory of Geomechanics and Embankment Engineering, Ministry of Education, Hohai University, Nanjing 210098, China;
2. College of Civil and Transportation Engineering, Hohai University, Nanjing 210098, China;
3. College of Mechanics and Materials, Hohai University, Nanjing 210098, China;
4. CCCC Tunnel Engineering Company Limited, Beijing 100102, China;
5. CRISMAT-ENSICAEN (UMR-CNRS 6508), Université de Caen-Basse-Normandie, Caen, F-14050, France;
6. China Railway 14th Bureau Group Co., Ltd., Jinan 250101, China

Received 4 June 2021; accepted 20 January 2022

Abstract: WC powders were uniformly coated by Ni nanoparticles through a combined chemical co-precipitation and subsequent high temperature hydrogen reduction strategy (abbreviated as CM-WCN), and then were consolidated by vacuum sintering at 1450 °C for 1 h to obtain WC−Ni cemented carbides. The microstructure and properties of the as-consolidated CM-WCN were investigated. The average grain size of WC in the consolidated CM-WCN was calculated to be in the range of 3.0−3.8 μm and only few pores were observed. A relative density of 99.6%, hardness of HRA 86.5 and bending strength of 1860 MPa were obtained for the CM-WCN−10wt.%Ni, and the highest impact toughness of 6.17 J/cm^2 was obtained for the CM-WCN−12wt.%Ni, surpassing those of the hand mixed WC−Ni (HM-WCN) cemented carbides examined in this study and the other similar materials in the literature. CM-WCN cemented carbides possess excellent mechanical properties, due to their highly uniform structure and low porosity that could be ascribed to the intergranular-dominated fracture mode accompanied by a large number of plastic deformation tears of the bonding phase. In addition, the corrosion resistance of CM-WCN was superior to that of HM-WCN at the Ni content of 6−12 wt.%.

Key words: WC−Ni cemented carbides; chemical co-precipitation method; high temperature hydrogen reduction strategy; Ni content; microstructure; impact toughness; corrosion resistance

1 Introduction

Cemented carbides are tool materials known as “industrial teeth” with a high hardness, strength and good wear resistance that are used to manufacture cutting tools, cutters, wear-resistant and corrosion-resistant parts [1−3]. They are sintered from a hard phase (such as WC and TiC) and a binder phase (such as Co, Ni, Fe or alloys). The hard phase directly determines the hardness, wear resistance and other characteristics of the alloy [4,5], whereas the metal phase is used to produce plastic flow at a high temperature to bond the hard phase. Although Co is most wildly used for the metal phase due to its excellent wettability to WC, the poor oxidation resistance and corrosion resistance of WC−Co cemented carbides still hinder their applications [6]. In addition, Co is a strategic scarce resource and is becoming increasingly expensive [7,8].

Corresponding author: Jian-feng ZHANG, Tel/Fax: +86-25-83787865, E-mail: jfzhang_sic@163.com
DOI: 10.1016/S1003-6326(22)65920-X

The uniform mixing of WC with the binder phase powders is the basis for the fabrication of cemented carbides with excellent performance. Typically, WC and Co powders are ball-milled for dozens of hours at a certain ball-to-powder mass ratio using ethanol or gasoline as a wet grinding medium [9,10]. Although this process has advantages such as high efficiency and easy operability, the severe damage of the WC powder morphology induces particle breakage and lattice distortion. Additionally, it is usually difficult to achieve uniform mixing of the powders due to the upper/lower delamination of the powders by the common planetary or roller ball milling [11].

Other candidate methods for mixing the cemented carbide powders such as electroless plating [12], spray [13], hydrothermal pressure hydrogen reduction [14] and chemical coprecipitation have been investigated. In particular, the chemical co-precipitation method has advantages of coating uniformity and a short synthesis cycle. SU et al [15] used a one-step reduction method to prepare a Co-coated WC powder, and the ultra-coarse grained WC−8wt.%Co cemented carbides were successfully consolidated. WANG et al [16] used ammonium tungstate and cobalt nitrate as raw materials, calcined them after chemical precipitation, and then directly reduced and carbonized the product in vacuum atmosphere to produce ultrafine WC−Co composite powders.

Similar to Co, Ni is a 3d element. Its mass, atomic radius, melting point, and physical properties are also similar to those of Co, and it is more abundant and its price is lower than that of Co. In addition, the corrosion and oxidation properties of Ni are clearly superior to those of Co [17,18]. Therefore, Ni is also expected to wet WC hard phases and form high performance WC−Ni cemented carbides. Despite the several studies on the WC−Ni composites reported in Refs. [19−22], the uniform dispersion of WC and Ni is still a key issue for the fabrication of high performance cemented carbides.

In this study, Ni nanoparticles were coated on the surface of WC (CM-WCN) by a chemical co-precipitation reaction process followed by hydrogen reduction, where WC was used as the nucleating agent and Ni salt was used as the precursor. Then, the composite powders were consolidated to obtain bulk cemented carbides. The sintering behavior, mechanical properties and corrosion resistance of the WC were investigated, and the sintering mechanism was discussed.

2 Experimental

2.1 Preparation of mixed powders

The raw materials used here involved WC powder (average diameter of 4.8−5.2 μm), hydrofluoric acid (40.0%), nitric acid (65.0%−68%) and $(NH_4)_2C_2O_4·H_2O$ (purity ≥ 99.5%). Figure 1 shows the flow chart for the fabrication of CM-WCN powders. Pure WC powder (50 g) was immersed in a mixed roughening solution (500 mL) with HF (0.67 mol/L) and HNO_3 (0.46 mol/L), and stirred for 30 min for fully coarsening.

For the co-precipitation process, the coarsened WC powder was poured into a $NiCl_2$ solution heated to 50 °C in a water bath and mechanically stirred for 20 min. Then, $(NH_4)_2C_2O_4$ solution was added into the $NiCl_2$ solution with scattered WC at a certain rate using the laboratory electric circulating pump, and the mixture was heated in a water bath and mechanically stirred for 30 min. The chemical co-precipitation reaction process is described by

$$NiCl_2·6H_2O+(NH_4)_2C_2O_4·H_2O= NiC_2O_4·2H_2O↓+2NH_4Cl+5H_2O \quad (1)$$

Then, the WC−Ni composite powders were obtained by calcining the mixed precursor in a H_2 atmosphere at 500 °C for 2 h as described by

$$2NiC_2O_4·2H_2O+5H_2= 2Ni+CO_2↑+3CO↑+7H_2O \quad (2)$$

For comparison, the WC−Ni composite powders were also prepared by hand mixing of WC and Ni powders (particle size of 1 μm). The mixed WC−Ni powders, with different Ni contents of 6, 8, 10, 12 and 14 wt.% were poured into an agate mortar. Meanwhile, anhydrous ethanol was added as a wet grinding medium, and wet grinding was carried out with the grinding pestle at a certain speed for 8 h for minimizing the variation of WC powder and dispersing Ni powder [23].

2.2 Consolidation of WC−Ni cemented carbides

The SDE molding agent (Zhuzhou Hetang Tengfei Cemented Carbide Forming Agent Co., Ltd., China) was added to the composite powders for blending and granulation, and then the powders

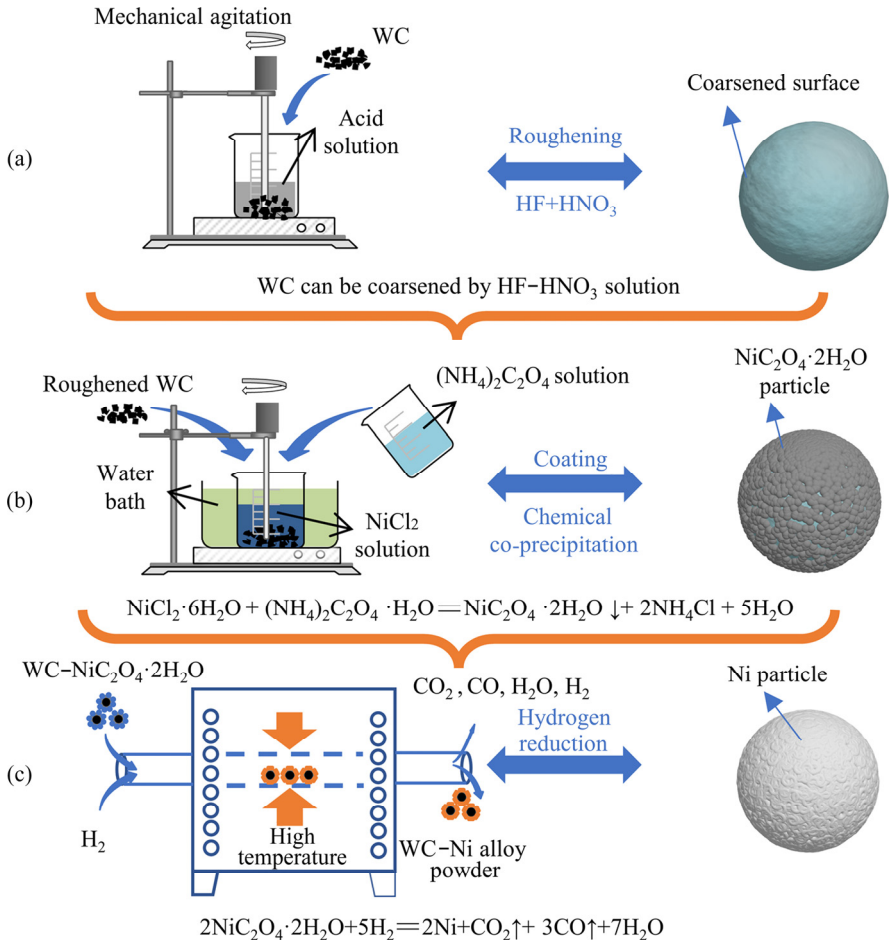

Fig. 1 Flow chart for fabrication of CM-WCN powders: (a) Roughening of WC; (b) Chemical co-precipitation; (c) High temperature hydrogen reduction

were pressed uniaxially at a pressure of 150 MPa. During the sintering process, the furnace (SF350, Zhuzhou Diyuan Powder Metallurgy Furnace Co., Ltd., China) was firstly heated from room temperature to 200 °C at a rate of 3 °C/min and held for 0.5 h, and heated to 470 °C at a rate of 2 °C/min and held for 1.5 h; then heated at 6 °C/min to 900 °C and held for 0.5 h, and heated to 1250 °C at a rate of 7 °C/min and held for 0.5 h; finally heated to 1450 °C at 2.5 °C/min and held for 1 h.

2.3 Microstructure and performance test

X-ray diffractometry (XRD, D8 Advance, Bruker, America) and scanning electron microscopy (SEM, EVO18, ZEISS, Germany) were used to analyze the phase composition, microstructure and bending fracture morphology. The linear intercept method was used to measure the WC grain size on the straight line in SEM images [24], and the average grain size of WC was obtained by measuring no less than 500 grains.

The relative density of alloy samples was measured directly using a density meter based on the Archimedes' method. The Rockwell hardness was measured using a digital Rockwell hardness tester with loading force of 588 N (Xi'an Huayin Instrument Equipment Co., Ltd., China). The impact toughness was measured using a pendulum testing machine (JB−6, Wuzhong Material Testing Machine Co., Ltd., China). The bending strength was measured using a universal testing machine (Jinan Nake Industry and Trade Co., Ltd., China) and calculated as follows according to the three-point test bending formula:

$$R=3FL/(2bh^2) \quad (3)$$

where R is the bending strength, F is the failure load, L is the sample span, b is the sample width, and h is the sample thickness.

The polarization curve and AC impedance of the alloy were measured using a three-electrode test system in a Chi660e electrochemical workstation. 1.0 mol/L NaCl solution was used as the corrosion solution. The self-corrosion current density (J_{corr})

and self-corrosion potential (φ_{corr}) of the alloy were analyzed using the analysis software of Chi660e electrochemical workstation. The corresponding equivalent circuit (electrochemical polarization) was selected by the software to fit the obtained AC impedance diagram, and the polarization resistance of the alloy was obtained.

3 Results and discussion

3.1 Powder mixing and hydrogen reduction

Figure 2 shows the micromorphology of the

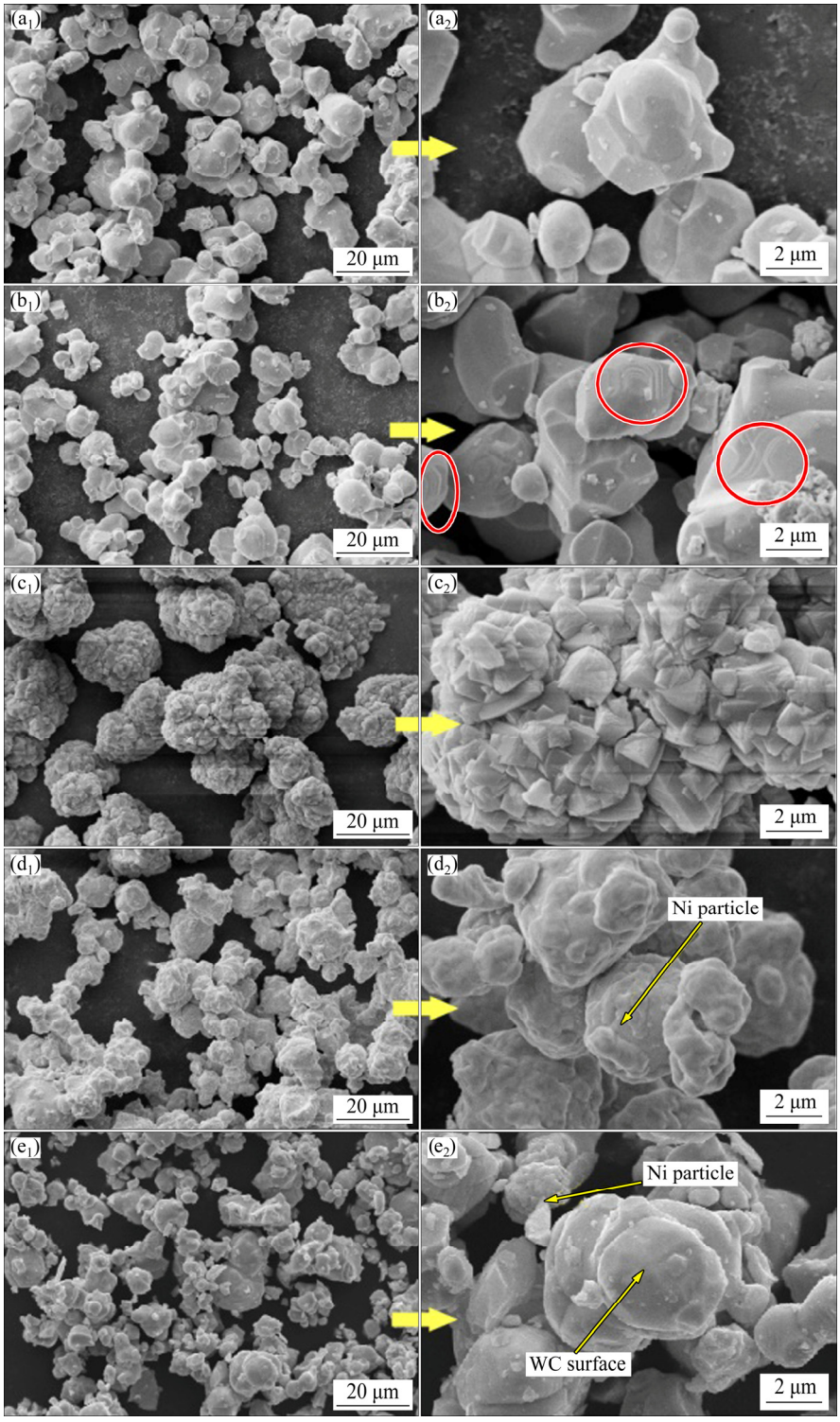

Fig. 2 SEM images of powders at different stages for fabrication of CM-WCN powders: (a_1, a_2) WC powder; (b_1, b_2) WC powder after coarsening; (c_1, c_2) WC−$NiC_2O_4·2H_2O$ composite powder; (d_1, d_2) CM-WCN composite powder; (e_1, e_2) HM-WCN composite powder

coated powders at each stage for the fabrication of CM-WCN powders. The original WC powder with a particle size of approximately 5 μm exhibits a smooth surface and a near-spherical grain with irregular shape (Figs. 2(a_1, a_2)). By contrast, gullies and step depressions appear on the coarsened powder surface due to the erosion by a strong acid solution (Figs. 2(b_1, b_2), marked by red circles) that makes the $NiC_2O_4·2H_2O$ particles obtained from the co-precipitation reaction attach more easily and uniformly to the WC surface (Fig. 2(c_1, c_2)). After placement in the hydrogen atmosphere at a high temperature of 500 °C for 1 h, the WC−$NiC_2O_4·2H_2O$ composite powder was reduced to the WC−Ni composite powder (Figs. 2(d_1, d_2)) that shows clear Ni coating on WC particles. The micromorphology of the HM-WCN sample is shown in Figs. 2(e_1, e_2). The morphology of the WC particles in the composite powder prepared by this method is irregular, and the particle surface of WC is clearly visible, indicating that the Ni phase distribution is highly uneven and a low-density of the Ni phase is obtained on the surface of WC particles. As shown in Fig. 3, the Ni particles prefer to agglomerate between WC particles, instead of dispersing on the surface of WC particles.

To confirm the coating uniformity of the $NiC_2O_4·2H_2O$ particles on the surface of WC, energy dispersive X-ray spectroscopy (EDS) element distribution mapping was carried out, and the results are shown in Fig. 4. Figure 4 shows that the powder is pure and no impurity elements are introduced. The distributions of W, C and O (Figs. 4(c−e)) are consistent with the SEM micrograph of the powder (Fig. 4(a). This shows that the coating of $NiC_2O_4·2H_2O$ powder on the surface of WC powder was successfully realized by the chemical co-precipitation process, and the particles of the coated $NiC_2O_4·2H_2O$ are evenly distributed.

Furthermore, Fig. 5 shows the XRD patterns of mixed powders in different stages of the fabrication of the CM-WCN powders. The precursor of the WC−Ni salt mixture obtained using the chemical co-precipitation reaction was identified to be $NiC_2O_4·2H_2O$, and no other impurity phases are observed (Fig. 5(c)). After hydrogen reduction, Ni peaks are clearly identified in addition to the WC peaks.

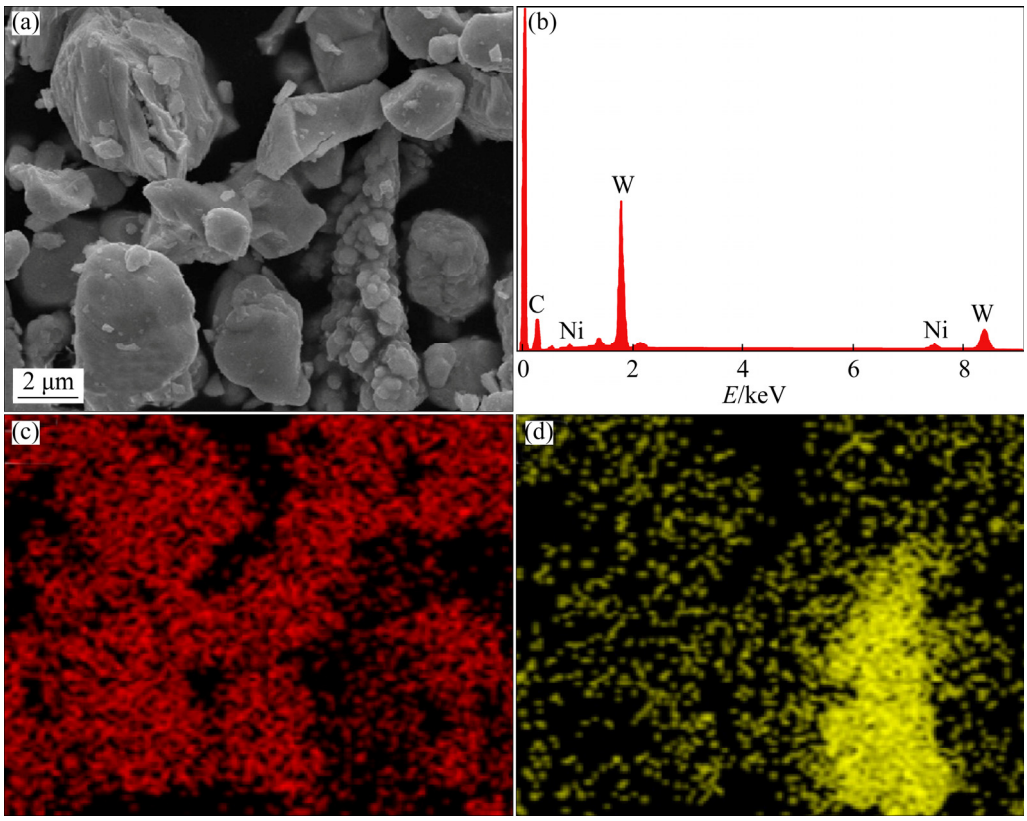

Fig. 3 SEM (a) and EDS mapping (b−d) images of WC−Ni composite powder obtained by hand mixing: (a) WC−Ni composite powder; (b) EDS spectrum; (c) W element distribution; (d) Ni element distribution

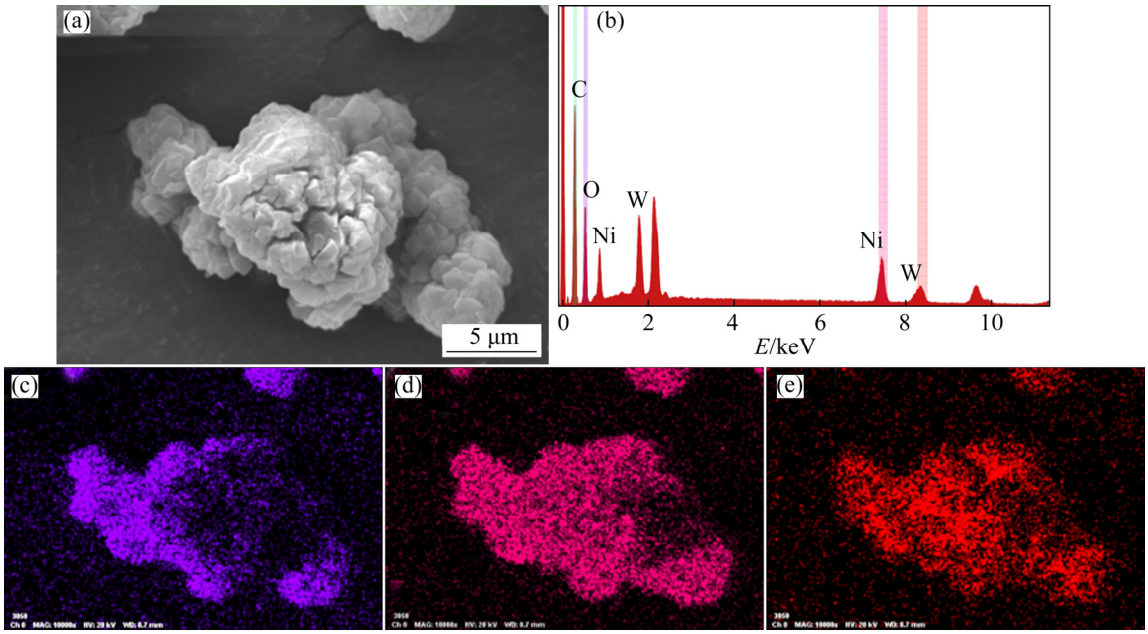

Fig. 4 SEM (a) and EDS mapping (b−e) images of WC−$NiC_2O_4·2H_2O$ composite powder: (a) Precursor powder; (b) EDS spectrum; (c) O element distribution; (d) Ni element distribution; (e) W element distribution

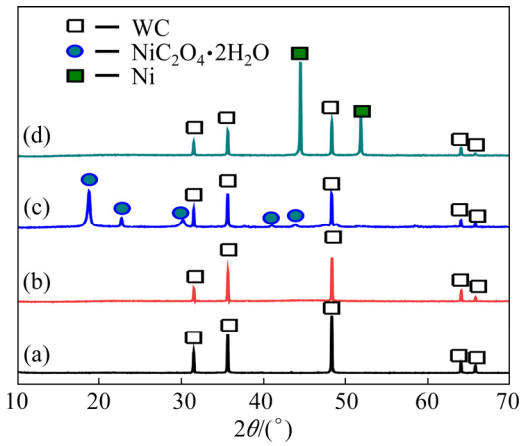

Fig. 5 XRD patterns of powders at different stages: (a) WC powder; (b) WC powder after coarsening; (c) WC−$NiC_2O_4·2H_2O$ composite powder; (d) CM-WCN composite powder

3.2 Sintering behavior

Figure 6 shows the effect of Ni content on the volume shrinkage and relative density of CM-WCN and HM-WCN. At the same Ni content, the sintering volume shrinkage of CM-WCN cemented carbide is higher than that of HM-WCN (Fig. 6(a)), suggesting that the chemical co-precipitation combined with hydrogen reduction is more beneficial to the densification than hand mixing. Figure 6(b) also shows that the relative density of CM-WCN is clearly higher than that of

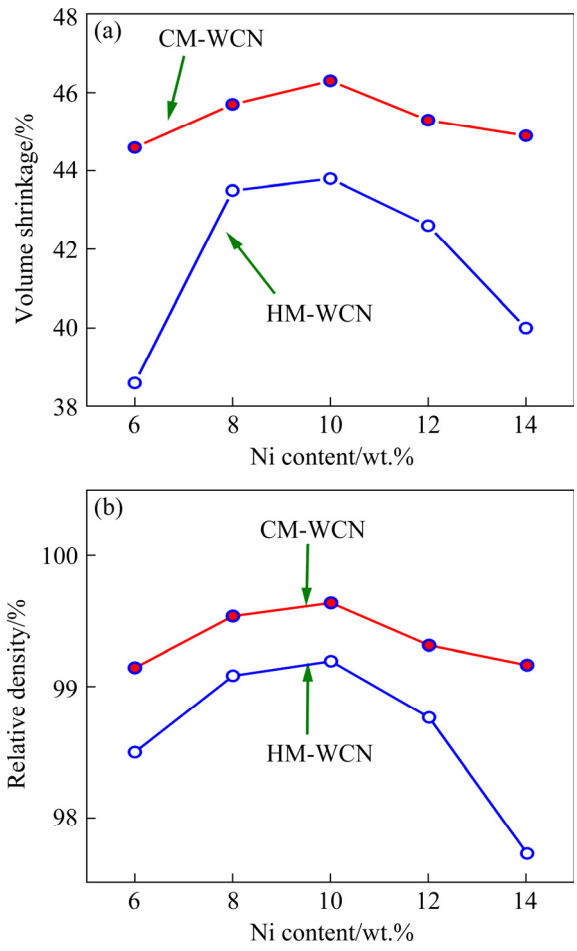

Fig. 6 Effect of Ni content on properties of CM-WCN and HM-WCN: (a) Volume shrinkage; (b) Relative density

HM-WCN, confirming the beneficial effects of the chemical co-precipitation combined with hydrogen reduction for the preparation of the WC and Ni mixed powders. The maximum relative density of CM-WCN was 99.6 %, higher than that of HM-WCN (99.2%) at Ni content of 10 wt.%.

The surfaces of CM-WCN and HM-WCN cemented carbide samples with different nickel contents manufactured by the two processes were polished and corroded for metallographic observation with the results shown in Fig. 7. For the Ni content of 6 wt.%, the holes are more clearly

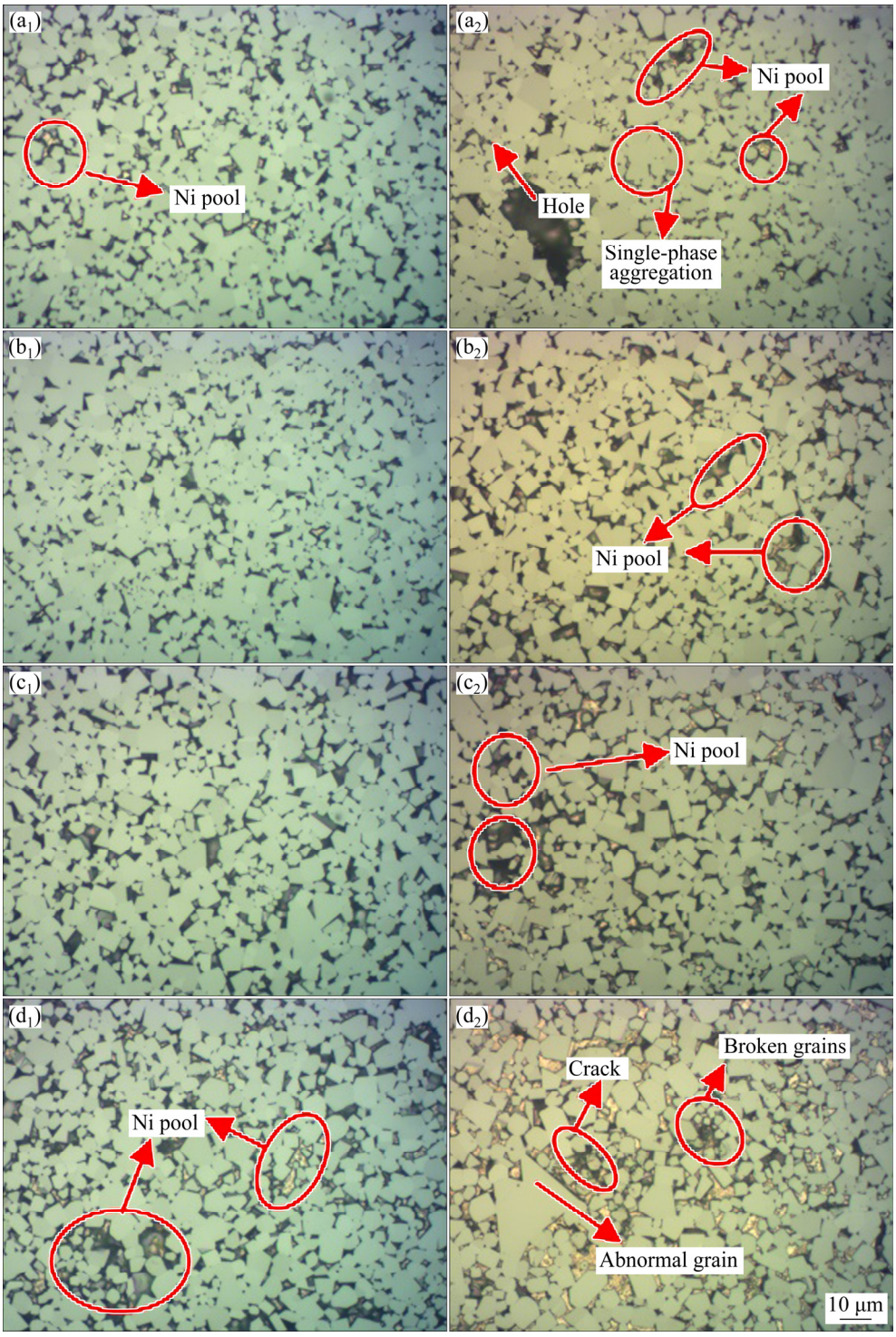

Fig. 7 Metallographic images of CM-WCN and HM-WCN: (a_1) CM-WCN−6wt.%Ni; (b_1) CM-WCN−10wt.%Ni; (c_1) CM-WCN−12wt.%Ni; (d_1) CM-WCN−14wt.%Ni; (a_2) HM-WCN−6wt.%Ni; (b_2) HM-WCN−10wt.%Ni; (c_2) HM-WCN−12wt.%Ni; (d_2) HM-WCN−14wt.%Ni

observed in HM-WCN than in CM-WCN. With an increase of the Ni content to 10 wt.% and 14 wt.%, the concentrations of defects and pores are greatly reduced both for HM-WCN and CM-WCN. However, abnormal grain growth of WC is clearly observed in HM-WCN due to the non-uniform mixing of WC and Ni by hand mixing. Moreover, some Ni pools are also found in HM-WCN and CM-WCN with Ni content of 14 wt.% probably arising from the aggregation of some Ni and WC grains, which contribute to the decreasing of relative density.

Figure 8 shows the WC grain size distribution and average grain size results for HM-WCN and CM-WCN. Both HM-WCN−10wt.%Ni and CM-WCN−10wt.%Ni are coarse cemented carbides (2.5−5.0 μm). The average grain size of HM-WCN is slightly larger due to the abnormal grain growth in this sample as shown in Fig. 7(c_2). The growth of the WC grains in cemented carbide is mainly due to either aggregation recrystallization or liquid recrystallization [25,26]. The aggregation recrystallization mainly occurs in the early phase of solid-phase sintering. Due to diffusion, the grain boundary between the WC particles disappears and large WC grains are formed. However, in the hand-mixing process, the grain surface distortion is higher and leads to easy aggregation. The surface distortion energy of CM-WCN composite powder produced by chemical co-precipitation and hydrogen reduction process is low, and Ni can be uniformly wrapped on the surface of WC, hindering the aggregation of WC to a certain extent and promoting its uniform growth of its grain.

Hence, in this case, both the hindered Ni diffusion and grain growth mainly controlled by aggregation recrystallization may lead to slowly shrinkage and grain growth. LIU et al [27] reported that the density did not increase any more when the binder content increased to 12 wt.% and 14 wt.%. It

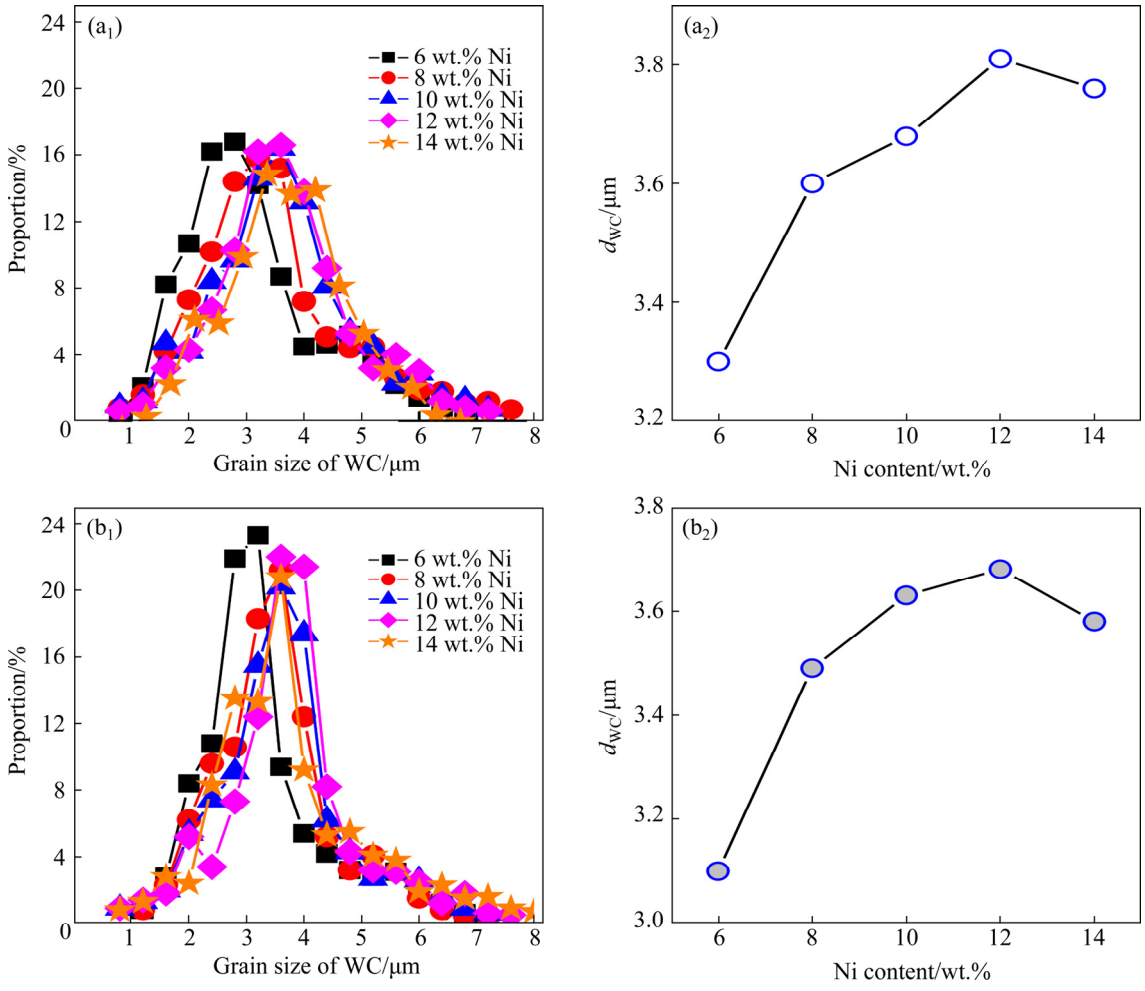

Fig. 8 WC grain size distribution (a_1, b_1) and average grain size (d_{WC}) (a_2, b_2) diagrams of HM-WCN (a_1, a_2) and CM-WCN (b_1, b_2)

is convinced that both density and grain size no longer significantly increased when the liquid phase reached a certain amount and its dispersion become worsen. And the variation of HM-WCN is more obvious.

3.3 Mechanical properties

Figure 9 shows the effect of Ni content on the mechanical properties of CM-WCN and HM-WCN.

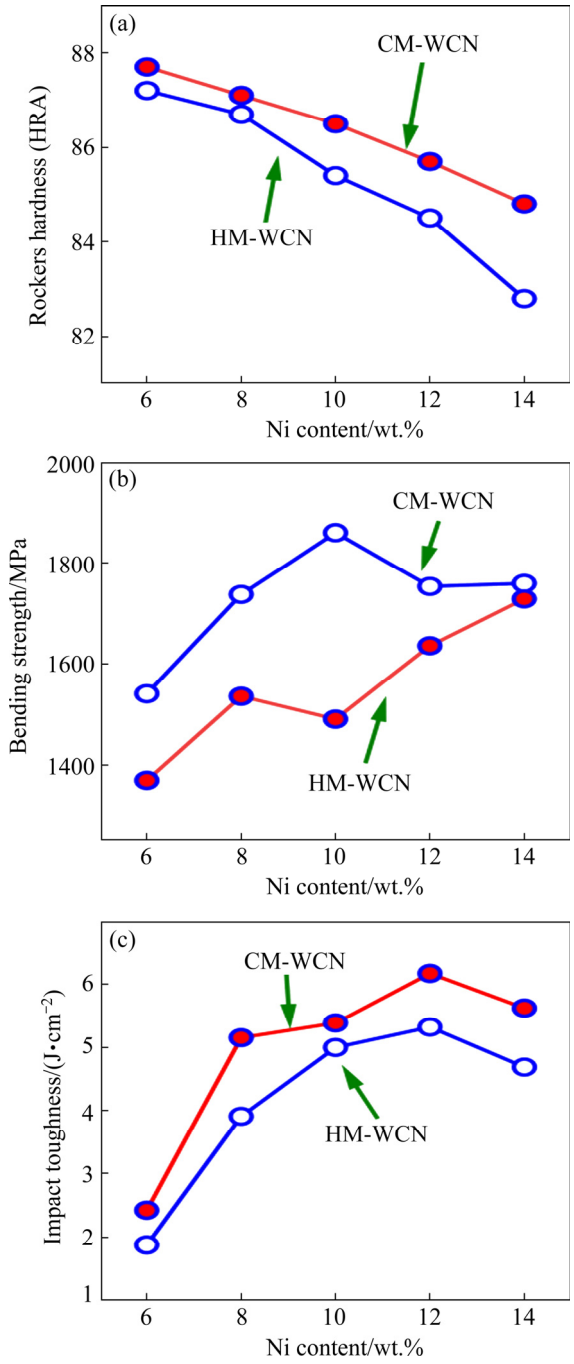

Fig. 9 Effect of Ni content on mechanical properties of CM-WCN and HM-WCN: (a) Rockers hardness; (b) Bending strength; (c) Impact toughness

With increasing Ni content, the hardness of cemented carbides tends to decrease, but the hardness of CM-WCN was clearly higher than that of HM-WCN. For example, the hardness of CM-WCN−10wt.%Ni was measured to be HRA 86.5, which is HRA 1.1 higher than that of HM-WCN−10wt.%Ni. The bending strength of CM-WCN−10wt.%Ni exhibits a maximum value of 1860 MPa, which is approximately 350 MPa higher than that of HM-WCN−10wt.%Ni. Furthermore, the impact toughness of CM-WCN−12wt.%Ni was measured to be 6.17 J/cm^2 and was also higher than that of HM-WCN−12wt.%Ni (5.33 J/cm^2) and was also higher than the impact toughness (5.0−6.0 J/cm^2) of the cutter alloy provided by some mainstream shield cutter suppliers domestically and abroad [28], validating the beneficial effects of the present chemical co-precipitation and hydrogen reduction strategy for mixing WC with Co.

It has been proposed that the performance degradation of cemented carbides is related to the formation of binder metal pool and micropores during the sintering process [29,30]. For an appropriate metal content and a uniform distribution of the metal (CM-WCN), the pores between the WC particles will be filled. By contrast, the metal pool or pores will appear for materials with a low or too high content of Ni (HM-WCN), reducing the density of the sintered alloy and giving rise to the degradation of mechanical properties.

Figure 10 shows the SEM images of the fracture surfaces of CM-WCN and HM-WCN. As observed from Fig. 10(a_1), the WC grain size of the alloy is relatively small and the main intergranular fracture mode is accompanied by a large number of plastic deformation tears of the binder phase. The enhanced WC grains formed in uniform binder structure of CM-WCN with low Ni content were main force against the fracture and the thickened binder phase may offer higher crack resistance than WC grains with increasing the Ni content. And the binder phase structure becomes more uniform and has higher fracture resistance when the Ni was 10 wt.%, resulting in the highest bending strength. For coarse-grained cemented carbides, the bending strength is proportional to hardness that is affected by WC grains size [31]. The WC grain size also increases with increasing the Ni content to 12 wt.%, while the coarse grains and abnormal grains increase, thus reducing hardness and the bending

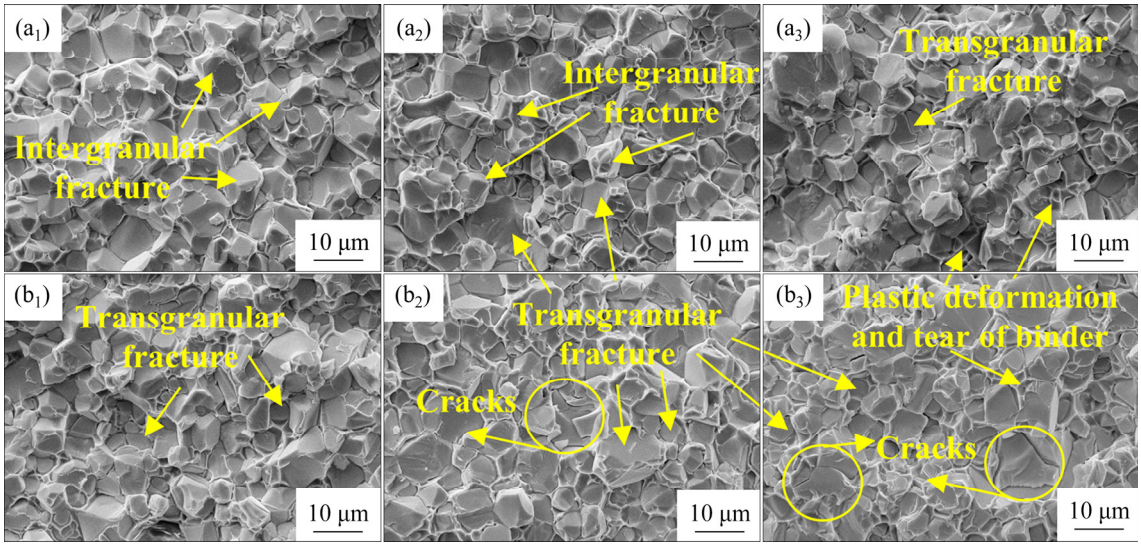

Fig. 10 SEM images of fracture surfaces of CM-WCN and HM-WCN: (a_1) CM-WCN−6wt.%Ni; (a_2) CM-WCN−10wt.%Ni; (a_3) CM-WCN−12wt.%Ni; (b_1) HM-WCN−6wt.%Ni; (b_2) HM-WCN−10wt.%Ni; (b_3) HM-WCN−12wt.%Ni

strength. Therefore, in alloy with higher Ni content, a small amount of transgranular mode is found in Fig. 10(a_2) and increases in Fig. 10(a_3) as abnormal WC grains have weak strength. This explains the much higher bending strength of CM-WCN−10wt.% Ni alloy compared to that of the CM-WCN−6wt.% Ni and CM-WCN−12wt.%Ni alloys. Furthermore, the CM-WCN−12wt.%Ni alloy has higher impact toughness as some coarse WC grains may absorb more work of fracture than fine grains.

However, an examination of Figs. 10(b_1), (b_2) and (b_3) shows that the main fracture mode of HM-WCN is the transgranular mode with a small amount of intergranular mode and tearing of the binder phase, exhibiting obvious brittle peeling with pores duo to weak strength of WC/WC interfaces. And those WC/WC interfaces and micropores in HM-WCN alloys may expedite the crack growth. Those defects found in HM-WCN−6wt.%Ni alloy may induce more transgranular features on the facture surface and decrease with increasing the Ni content. Although the WC−Ni structure of the HM-WCN alloys with high Ni content is improved, more abnormal WC grains are generated and the cracks inside those grains with defects extend into the alloy on the fracture surfaces of those HM-WCN alloys. Therefore, compared with CM-WCN alloys, the HM-WCN alloys have more uneven WC−Ni structure, poorer density and coarser WC grains with more defects, resulting in lower bending strength and impact toughness.

3.4 Corrosion resistance

The obtained polarization curves of CM-WCN and HM-WCN are shown in Fig. 11, and the electrochemical corrosion parameters derived from the polarization curves are supplied in Table 1. Here, the corrosion resistance was evaluated using the polarization resistance (R_p) and the self-corrosion current density (J_{corr}). A lower self-corrosion current density corresponds to the greater polarization resistance and corrosion resistance of the cemented carbide [32−34]. At the same time, in the electrochemical reaction, a higher J_{corr} implies a higher oxidation reaction equilibrium constant and a higher oxidation rate [35,36]. For a given Ni content (except for the Ni content of 14 wt.%), the J_{corr} of CM-WCN is smaller than that of HM-WCN, while the R_p value is larger, indicating the superior corrosion resistance of CM-WCN compared to that of HM-WCN. This may be ascribed to the more uniform distribution of Ni nanoparticles on WC in CM-WCN. And the corrosion resistance of CM-WCN is also found to be better than the reported value of WC−Co cemented carbides in Refs. [32,37].

An examination of the data in Table 1 shows that the corrosion resistance of the alloy prepared by the two processes does not increase monotonically with increasing Ni content, but reaches a peak at the Ni content of 10 wt.% for CM-WCN and a peak at the Ni content of 12 wt.% for HM-WCN, and then decreases with further increase in Ni content. Deteriorated corrosion may

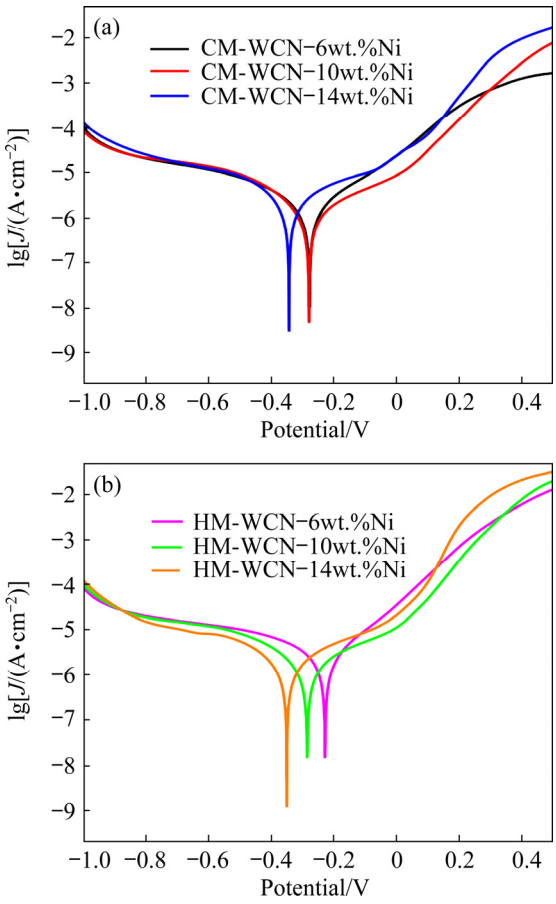

Fig. 11 Polarization curves of cemented carbides: (a) CM-WCN; (b) HM-WCN

Table 1 Electrochemical corrosion performance of cemented carbides

Alloy	J_{corr}/ (A·cm^{-2})	φ_{corr}/ V	R_p/ (Ω·cm^2)
CM-WCN−6wt.%Ni	1.517×10^{-6}	−0.277	27592.7
CM-WCN−8wt.%Ni	1.749×10^{-6}	−0.300	25055.0
CM-WCN−10wt.%Ni	1.164×10^{-6}	−0.270	35838.4
CM-WCN−12wt.%Ni	1.165×10^{-6}	−0.272	34357.0
CM-WCN−14wt.%Ni	2.238×10^{-6}	−0.343	20725.3
HM-WCN−6wt.%Ni	2.342×10^{-6}	−0.228	18561.5
HM-WCN−8wt.%Ni	2.330×10^{-6}	−0.322	19164.5
HM-WCN−10wt.%Ni	1.422×10^{-6}	−0.285	30336.6
HM-WCN−12wt.%Ni	1.242×10^{-6}	−0.282	31039.0
HM-WCN−14wt.%Ni	1.516×10^{-6}	−0.350	28790.9

be caused by the decreasing of density and the grain boundary structure. LIU et al [38] reported that higher hardness can improve the corrosion resistance, which may be another reason for the reduced corrosion resistance when Ni content exceeds a certain value. Furthermore, as shown in Table 1, the corrosion resistance of HM-WCN has excellent improvement with increasing the Ni content to 12 wt.% as the effect of uniformity of WC−Ni structure becomes weak. When the Ni content reaches 14 wt.%, the HM-WCN shows better corrosion resistance than CM-WCN. This may be related to the internal corrosion from the pores. The pores in CM-WCN and HM-WCN alloys are different: one type of small approximately equiaxed pores and one type of larger elongated pores, respectively [39]. It is clear that the equiaxed interior pores may expose more WC−Ni interfaces for quickly forming the electrochemical reaction, resulting in the acceleration of internal corrosion of alloy, whereas for HM-WCN the larger elongated pores may hinder the invasion of corrosive liquid by WC/WC boundaries, resulting in the superior corrosion resistance with the Ni content of 14 wt.%.

4 Conclusions

(1) As shown by the microstructural observation, the CM-WCN exhibited decreased porosity and defect concentration.

(2) Due to the uniform distribution of Ni nanophase, low porosity and enhanced WC grains, relative density of 99.6%, hardness of HRA 86.5 and bending strength of 1860 MPa were obtained for the CM-WCN−10wt.%Ni, and high impact toughness of 6.17 J/cm^2 was obtained for the CM-WCN−12wt.%Ni, surpassing those of HM-WCN cemented carbides examined in this study.

(3) Due to the uniform addition of Ni, CM-WCN with the Ni contents of 10 wt.% and 12 wt.% exhibited a superior corrosion resistance. Therefore, the CM-WCN cemented carbides fabricated in this study are promising materials for use in engineering applications.

Acknowledgments

The authors would like to acknowledge the financial supports from the National Natural Science Foundation of China (Nos. 51778213, 52078189), and the Fundamental Research Funds for the Central Universities, China (No. B200202073).

References

[1] ORTNER H M, ETTMAYER P, KOLASKA H, SMID I. The history of the technological progress of hardmetals [J]. International Journal of Refractory Metals and Hard Materials, 2014, 48: 148−159.

[2] LIN N, HE Y H, ZOU J. Enhanced mechanical properties and oxidation resistance of tungsten carbide−cobalt cemented carbides with aluminum nitride additions [J]. Ceramics International, 2017, 43: 6603−6606.

[3] LI X G, YUAN D J, JIANG X Q, WANG F. Damages and wear of tungsten carbide-tipped rippers of tunneling machines used to cutting large diameter reinforced concrete piles [J]. Engineering Failure Analysis, 2021, 127: 105533.

[4] LI J F, CHENG J G, CHEN P Q, CHEN W C, WEI C L. Fabrication of WC−Co cemented carbides with gradient distribution of WC grain size and Co composition by lamination pressing and microwave sintering [J]. Ceramics International, 2018, 44: 11225−11232.

[5] YANG Q M, YANG J G, YANG H L, RUAN J M. The effects of fine WC contents and temperature on the microstructure and mechanical properties of inhomogeneous WC-(fine WC−Co) cemented carbides [J]. Ceramics International, 2016, 42: 18100−18107.

[6] HAMID Z A, EL BADRY S A, AAL A A. Electroless deposition and characterization of Ni−P−WC composite alloys [J]. Surface and Coatings Technology, 2007, 201: 5948−5953.

[7] SUN J L, ZHAO J, HUANG Z F, YAN K, SHEN X H, XING J D, GAO Y M, JIAN Y X, YANG H J, LI B. A review on binderless tungsten carbide: Development and application [J]. Nano-Micro Letters, 2020, 12: 162−198.

[8] FERNANDES C M, SENOS A M R. Cemented carbide phase diagrams: A review [J]. International Journal of Refractory Metals and Hard Materials, 2011, 29: 405−418.

[9] MANDEL K, KRÜGER L, SCHIMPF C. Particle properties of submicron-sized WC−12Co processed by planetary ball milling [J]. International Journal of Refractory Metals and Hard Materials, 2014, 42: 200−204.

[10] QIAN C, LI K, GUO X Y, LIU B, LONG Z Y, LIU Y. Effect of WC grain size on mechanical properties and microstructures of cemented carbide with medium entropy alloy Co−Ni−Fe binder [J]. Journal of Central South University, 2020, 27: 1146−1157.

[11] SHEN J, SUN J F, ZHANG F M. Synthesis and characterizations of nanocrystalline WC−Co composite powders by a unique ball milling process [J]. Journal of Materials Science & Technology, 2004, 20: 7−10.

[12] GUO L, XIAO L R, ZHAO X J, SONG Y F, CAI Z Y, WANG H J, LIU C B. Preparation of WC/Co composite powders by electroless plating [J]. Ceramics International, 2017, 43: 4076−4082.

[13] WANG Q, CHEN Z H, LI L X, YANG G B. The parameters optimization and abrasion wear mechanism of liquid fuel HVOF sprayed bimodal WC−12Co coating [J]. Surface and Coatings Technology, 2012, 206: 2233−2241.

[14] ADORJAN C, BOCK A, MYLLMÄEKI S, SCHUBERT W D, KONTTURI K. WC/Co-composite powders via hydrothermal reduction of Co_3O_4-suspensions [J]. International Journal of Refractory Metals and Hard Materials, 2008, 26: 569−574.

[15] SU W, SUN Y X, WANG H F, ZHANG X Q, RUAN J M. Preparation and sintering of WC−Co composite powders for coarse grained WC−8Co hardmetals [J]. International Journal of Refractory Metals and Hard Materials, 2014, 45: 80−85.

[16] WANG Y X, WEN X Q, ZHOU J. Ultrafine WC−Co composite powder preparation by chemical precipitation method [J]. China Tungsten Industry, 2012, 27: 24−27. (in Chinese)

[17] SU W, WEN Y, ZHANG Q. Effects of Ni and Cu additions on microstructures, mechanical properties and wear resistances of ultra-coarse grained WC−6Co cemented carbides [J]. International Journal of Refractory Metals and Hard Materials, 2018, 70: 176−183.

[18] ZHANG W W, LUO B H, GAO Y, BAI Z H. Effects of Fe/Ni ratio on microstructure and properties of WC−Fe−Ni cemented carbide [J]. Transactions of Nonferrous Metals Society of China, 2018, 28: 1798−1807.

[19] CORREA E O, SANTOS J N, KLEIN A N. Microstructure and mechanical properties of WC Ni−Si based cemented carbides developed by powder metallurgy [J]. International Journal of Refractory Metals and Hard Materials, 2010, 28: 572−575.

[20] CHEN H Y, WANG Z C, LUO L M, ZHU L, TU Z B, WU Y C. Effect of Ni content on microstructure and properties of WC−Ni composites prepared by electroless plating and powder metallurgy [J]. Rare Metal Materials and Engineering, 2017, 46: 2820−2824.

[21] TARRAGÖ J M, FERRARI C, REIG B, COUREAUX D, SCHNEIDER L, LLANES L. Mechanics and mechanisms of fatigue in a WC−Ni hardmetal and a comparative study with respect to WC−Co hardmetals [J]. International Journal of Fatigue, 2015, 70: 252−257.

[22] SHI K H, ZHOU K C, LI Z Y, ZHANG D, ZAN X Q. Microstructure and formation process of Ni-pool defect in WC−8Ni cemented carbides [J]. Transactions of Nonferrous Metals Society of China, 2015, 25: 873−878.

[23] MIN F L, WANG X Y, LI M D, NI Y X, AL-QADHI E, ZHANG J F. Preparation of high-porosity and high-strength ceramisites from municipal sludge using starch and $CaCO_3$ as a combined pore-forming agent [J]. Journal of Materials in Civil Engineering, 2021, 33: 04020502.

[24] LIN C G, YUAN G S. Quantitative measure of WC grain size in nanocrystalline WC−Co hardmetal [J]. The Chinese Journal of Nonferrous Metals, 2005, 15: 823−828. (in Chinese)

[25] SOARES E, MALHEIROS L F, SACRAMENTO J, VALENTE M A, OLIVEIRA F J. Ethanol and water processing of submicrometer cemented carbide powders [J]. Journal of the American Ceramic Society, 2011, 94: 84−91.

[26] KIM S, PARK J K, LEE D. Effect of grain motion on the coarsening of WC grains in the carbon-saturated liquid matrix during liquid phase sintering of WC−Co alloys [J]. Scripta Materialia, 1998, 38: 1563−1569.

[27] LIU K, WANG Z H, YIN Z B, CAO L Y, YUAN J T. Effect

of Co content on microstructure and mechanical properties of ultrafine grained WC−Co cemented carbide sintered by spark plasma sintering [J]. Ceramics International, 2018, 44: 18711−18718.
[28] WANG W, LU Z C, ZENG M Q, ZHU M. Achieving combination of high hardness and toughness for WC−8Co hardmetals by creating dual scale structured plate-like WC [J]. Ceramics International, 2018, 44: 2668−2675.
[29] ZHANG S Q, CHENG D F, WANG H F, XIAO W. Evolvement of cobalt agglomerate during cemented carbide sintering process [J]. Materials Science and Engineering of Powder Metallurgy, 2010, 15: 661−666. (in Chinese)
[30] BAO R, GUO S D, YI J H, CHEN H, YANG J G, YU F. Microwave reaction sintering on WC−Co cemented carbides fabrication [J]. The Chinese Journal of Nonferrous Metals, 2020, 30: 1828−1836. (in Chinese)
[31] FANG Z Z. Correlation of transverse rupture strength of WC−Co with hardness [J]. International Journal of Refractory Metals and Hard Materials, 2005, 23: 119−127.
[32] ROCHA A M F, BASTOS A C, CARDOSO J P, RODRIGUES F, FERNANDES C M, SOARES E, SACRAMENTO J, SENOS A M R, FERREIRA M G S. Corrosion behaviour of WC hardmetals with nickel-based binders [J]. Corrosion Science, 2019, 147: 384−393.
[33] HUMAN A M, EXNER H E. Electrochemical behaviour of tungsten-carbide hardmetals [J]. Materials Science and Engineering A, 1996, 209: 180−191.
[34] SUTTHIRUANGWONG S, MORI G. Corrosion properties of Co-based cemented carbides in acidic solutions [J]. International Journal of Refractory Metals and Hard Materials, 2003, 21: 135−145.
[35] CHANG S H, CHEN S L. Characterization and properties of sintered WC−Co and WC−Ni−Fe hard metal alloys [J]. Journal of Alloys and Compounds, 2014, 585: 407−413.
[36] YEO S, KIM D J, PARK J W. Enhanced corrosion resistance of WC−Co with an ion beam mixed silicon carbide coating [J]. International Journal of Refractory Metals and Hard Materials, 2011, 29: 582−585.
[37] FAN B W, ZHU S G, DONG W W, DING H, BAI Y F, LUO Y L, DI P. Comparative study on corrosion behavior of WC−MgO composite and WC−6Co cemented carbide in NaCl solution [J]. Ceramics International, 2021, 47: 7106−7116.
[38] LIU J, BAI X Q, CHEN T Z, YUAN C Q. Effects of cobalt content on the microstructure, mechanical properties and cavitation erosion resistance of HVOF sprayed coatings [J]. Coatings, 2019, 9: 534.
[39] PETERSSON A, ÅGREN J. Rearrangement and pore size evolution during WC−Co sintering below the eutectic temperature [J]. Acta Materialia, 2005, 53: 1673−1683.

Ni 包覆 WC 粉体及高抗冲击耐腐蚀 WC−Ni 硬质合金的制备和性能

闵凡路[1,2]，于淞百[3]，汪 升[2]，姚占虎[4]，Jacques Guillaume NOUDEM[5]，刘四进[6]，张建峰[3]

1. 河海大学 岩土力学与堤坝工程教育部重点实验室，南京 210098；
2. 河海大学 土木与交通学院，南京 210098；
3. 河海大学 力学与材料学院，南京 210098；
4. 中交隧道工程局有限公司，北京 100102；
5. CRISMAT-ENSICAEN (UMR-CNRS 6508), Université de Caen-Basse-Normandie, Caen, F-14050, France;
6. 中铁十四局集团有限公司，济南 250101

摘 要：采用化学共沉淀−高温氢还原工艺制备纳米 Ni 均匀包覆的 WC 复合粉体(简称 CM-WCN)，在 1450 ℃下真空烧结 1 h，获得 WC−Ni 硬质合金，并对其组织及性能进行研究。结果表明，CM-WCN 硬质合金中 WC 的平均晶粒度为 3.0~3.8 μm，仅观察到少量孔隙。CM-WCN−10%Ni(质量分数)的相对密度、硬度及抗弯强度分别为 99.63%、HRA 86.5 及 1860 MPa，CM-WCN−12%Ni(质量分数)的最高冲击韧性为 6.17 J/cm^2，优于本文中手混法制备的 WC−Ni (HM-WCN)硬质合金及文献报道同类合金的性能。由于结构均匀性及低孔隙率，CM-WCN 硬质合金具有优异的力学性能，其主要断裂模式为穿晶断裂，并伴随黏结相塑性形变。此外，当 Ni 含量为 6%~12%(质量分数)时，CM-WCN 比 HM-WCN 硬质合金的耐腐蚀性能更好。

关键词：WC−Ni 硬质合金；化学共沉淀法；高温氢还原法；Ni 含量；显微组织；冲击韧性；耐腐蚀性

(Edited by Wei-ping CHEN)